Measurement and Analysis of Supraharmonic Emissions in Smart Grids

Deepak Amaripadath, Robin Roche, Loic Joseph-Auguste, Daniela Istrate, Dominique Fortune, Jean-Pierre Braun, Fei Gao

Measurement and Analysis of Supraharmonic Emissions in Smart Grids

Deepak Amaripadath, Robin Roche, Loïc Joseph-Auguste, Daniela Istrate, Dominique Fortuné, Jean-Pierre Braun, and Fei Gao

***Abstract*— This paper describes the design of a measurement system for supraharmonic emissions in the frequency range of 2 to 150 kHz, and analyzes the measurements obtained in real grid scenarios. The measurement system is first characterized in the laboratory. The Design of Experiment approach then uses an adequate number of experiments to identify the effects and interactions of factors responsible for supraharmonic emissions. For each of these experiments, the measured supraharmonic emissions are analyzed and quantified using the fast Fourier transform. Next, this data is studied using the Analysis of Variance method, which enables identifying the critical factors that generate supraharmonic emissions in the network. The measurement and analysis results show the individual effects and interactions between these factors.**

***Index Terms*—Analysis of variance, Photovoltaic systems, Smart grids, Power quality, Sensors, Signal processing algorithms.**

I. Introduction

THE ever growing presence of devices connected to the grid through power electronic converters, such as photovoltaic (PV) panels and batteries, as well as the development of power line communication (PLC), e.g., for smart metering, has led to the emergence of new power quality issues [1]. An example is those related to supraharmonics [2], limited to the frequency range of 2 to 150 kHz. The effects of supraharmonic emissions include capacitor overheating, electromagnetic incompatibility, and interference with power line communication (PLC) [2-6]. Overall, the increased integration of these non-linear loads can result in the deterioration of the power quality in the distribution grid [7,8]. As the share of renewables is growing steadily throughout the world, a better understanding of how these supraharmonic emissions behave and propagate is needed to support this development. This first requires being able to measure these emissions accurately, especially in the actual distribution grids, where these emissions are more random and unpredictable than in controlled environments [4].

This project has received funding from the European Union's Horizon 2020 research and innovation programme under Grant Agreement No. 676042.

D. Amaripadath, D. Istrate, and D. Fortune are with the Low Frequency Electrical Metrology Department, LNE, 29 avenue Roger Hennequin, 78197 Trappes, France (e-mail: deepak.amaripadath@lne.fr).

D. Amaripadath, R. Roche, and F. Gao are with FEMTO-ST, CNRS, Univ. Bourgogne Franche-Comté, UTBM, 90000 Belfort, France.

L. Joseph-Auguste is with Concept Grid, Lab Les Renardières, EDF, Avenue des Renardières, 77250 Moret-sur-Loing, France.

J.P. Braun is with the Electrical Energy and Power Laboratory, METAS, Lindenweg 50, CH-3003 Berne-Wabern, Switzerland.

Existing literature from [8,9,10] outlines the challenges in measuring supraharmonic emissions. The measurements require sensors with, at the same time, high accuracy, sensitivity, and wide bandwidth. The measurement system also requires high pass filtering for a better dynamic range. Studies from [6,11] uses a 2-channel measurement system with an oscilloscope. The voltage channel uses a high pass filter, which removes the fundamental component and measures only the supraharmonic emissions. Here, the voltage channel does not measure the fundamental component. In addition, the current sensor used for the measurements is sealed and is used on a reconfigurable site. However, this is usually not the case in public networks, so the current channel lacks flexibility for the grid measurements. Therefore, it is important to design a flexible measurement system considering safety aspects for actual grid measurements. Other existing studies describe the measurements, but do not explain the measurement system.

Analyzing the emission patterns and propagation of supraharmonics is a challenge, especially in the presence of multiple sources. The influencing factors and their respective impact are currently not well known and deserve further research. Supraharmonic emissions may be classified into primary and secondary emissions. The equipment under test generates primary emissions, whereas secondary emissions are generated by different equipment and then propagate towards the equipment under test due to low impedance of the equipment terminal [3]. For instance, according to [4], both simulation-based tests and field measurements confirm that the magnitude of the current flowing towards the grid at the switching frequency of the converter decreases with the increase in the number of similar equipment in the grid. This is studied using electric vehicle (EV) chargers of the same type with and without a PV installation. Emissions from individual equipment like PV inverters, in the presence of other household equipment like television, are outlined in [8]. Emissions at the equipment terminals can also be much higher than those at the delivery point [3], so the measurements should be performed at multiple points to obtain a correct representation of emission levels in the electrical network. Studies from [1-5] uses the fast Fourier transform (FFT) to quantify the supraharmonic emissions and short time Fourier transform (STFT) to analyze the time-frequency variations of the supraharmonic emissions.

For further development in this area, new studies involving electrical networks with multiple generation and load equipment are required. This would lead to a more comprehensive analysis of a real grid scenario involving the

interactions between different equipment and how they contribute individually to these interactions. In this paper, the individual effects and interactions between different equipment in the grid are studied using the Design of Experiment (DoE) approach. The DoE approach helps to cover the experimental space efficiently with a limited number of tests [12]. This approach also provides a cause and effect relationship between the different factors considered in the test, thereby creating a better understanding of the test results [13]. Here, a test network with different source and load equipment is configured with different measurement points.

This paper significantly extends the work presented in [14]. The main contribution of this paper is twofold. First, a measurement system is designed to measure the fundamental and supraharmonic components of both voltage and current waveforms separately. The characterization of measurement system is also described. Second, the DoE approach is used with a test network, considering the main factors that create supraharmonic emissions. The subsequent analysis of the measured waveforms is performed using two complementary techniques. A mathematical processing uses the FFT to quantify the emissions. Then, a statistical analysis uses the Analysis of Variance (ANOVA) to study the behavior and interactions of the different factors in the electrical grid.

II. Measurement System

A. Measurement system design

A system dedicated to the measurement of supraharmonic emissions is first designed and fabricated. The measurement system with its components is described in [14]. As shown in Fig. 1, channels 1 and 2 are dedicated for the voltage measurements and channels 3 and 4 are dedicated for the current measurements. These channels measure the fundamental and supraharmonic components separately in order to maximize the dynamic range of the recorder. The voltage transformer (VT) and voltage sensor unit (VSU) are used to measure the voltage waveforms, while the Rogowski coils (RC_1 and RC_2), which are non-invasive and wideband current sensors, are used to measure the current waveforms.

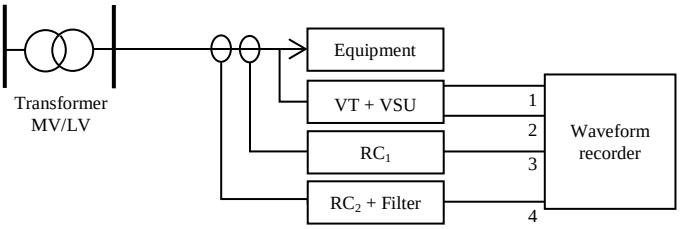

Fig. 1. Measurement system connection schema.

The 4-channel waveform recorder is used at a sampling rate of 1 MS/s, and voltage level up to ±25 V. The oscilloscope gain is adjusted for each channel separately during the measurements in order to maximize the resolution.

B. Measurement System Characterization

The measurement system was characterized to determine the frequency and amplitude response of the sensors. The waveform amplitudes are represented in root mean square (RMS) values. For the voltage sensors, the characterization principle relies on the comparison of the reference voltage from the generator and voltage indicated by a multimeter. The VT is characterized in the frequency range of 50 Hz to 30 kHz at 7V, and in the amplitude range of 50 mV to 230 V at 50 Hz. The VSU is characterized in the frequency range of 30 to 150 kHz at 3V and in the amplitude range of 25 mV to 7 V at 50 kHz. The current sensor characteristics with varying frequency and amplitude are summarized in Table I.

The current sensors are characterized [15] by comparing the RC output with a reference current transformer output, as shown in Fig. 2. The voltage waveform is converted to a current waveform by a radio frequency (RF) power amplifier and load impedance. The waveforms are measured by the sensors and the outputs are compared.

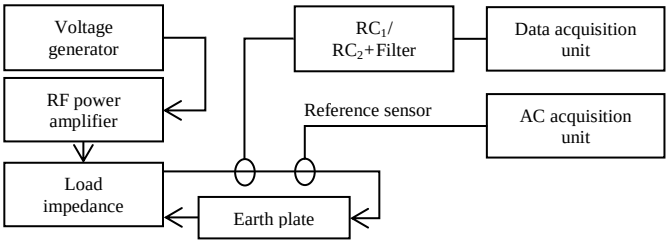

Fig. 2. Current sensor characterization schema.

A first order high pass filter is used with RC_2 to attenuate the fundamental component. The RC_1 sensor is characterized in the frequency range of 20 Hz to 150 kHz at 1 A, and in the amplitude range of 5 to 85 A at 50 Hz. The RC_2 with a first order high pass filter is characterized in the frequency interval of 2 to 150 kHz at 1 A, and in the amplitude range of 20 mA to 1 A at 5 kHz. The current sensor characteristics with varying frequency and amplitude are summarized in Table I.

TABLE I
Measurement System variations with Frequency and Amplitude.

Linearity error with varying frequency		
Sensor	**Frequency range (kHz)**	**Linearity Error (%)**
VT	0.05 - 30	0.83
VSU	30 - 150	0.62
RC_1	0.02 - 150	0.17
RC_2 + Filter	0.02 - 150	1.14
Linearity error with varying amplitude		
Sensor	**Amplitude range**	**Linearity Error (%)**
VT	0.05 - 230 V	0.32
VSU	0.025 - 7 V	0.84
RC_1	5 - 85 A	0.06
RC_2 + Filter	0.02 - 1 A	0.83

The sensitivity coefficients of the voltage and current sensors are used to convert the sensor outputs to voltage and current amplitudes, respectively. These values are then used for further analysis of supraharmonic emissions.

III. Design of Experiment

After the measurement system has been designed and correctly characterized, can be installed for obtaining real grid measurements on the Concept Grid platform of Electricité de France (EDF). Concept Grid is a test and validation platform

for smart grids described in [16,17]. The measurements are performed on the low voltage network side of the grid. Based on the existing literature in [2,4,18] and an analysis of the Concept Grid architecture, the factors that influence the generation of supraharmonic emissions are considered (see Table II): the connected generation (e.g., PV inverters) and load equipment, the measurement point location, and the modes of operation (High or Low).

TABLE II
TEST NETWORK FACTORS.

No.	Factors	Mode of operation	
A	Residential PV inverter (PVI_R)	High	Low
B	Industrial PV inverter (PVI_I)	High	Low
C	Residential load	High	Low
D	Measurement point	MP_1	MP_2

"High" represents operation in full capacity for the inverters and residential load, while "Low" represents the off state for the inverters and sole operation of light bulbs for the residential load. The measurement points are either at MP_1, which is closer to the residential load, or at MP_2, which is closer to the PV inverters, as shown in Fig. 3.

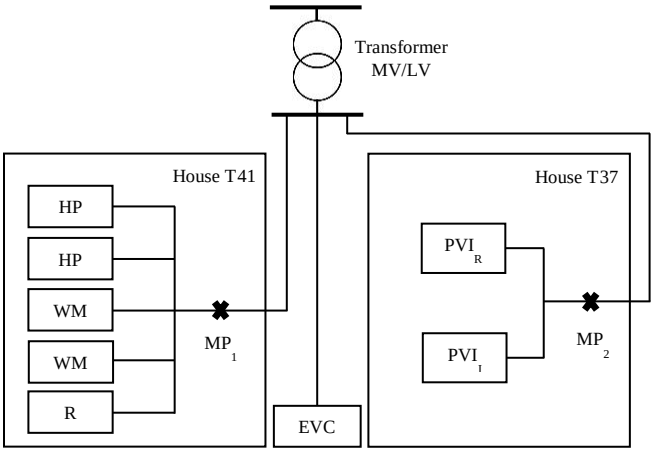

Fig. 3. Electrical network for real grid measurements [14].

The generation and load equipment used in the network and in Fig. 3 are as follows:

- HP is for heat pump;
- WM is for washing machine;
- R is for refrigerator;
- EVC is for electric vehicle charger;
- PVI_R is for residential PV inverter;
- PVI_I is for industrial PV inverter;
- MP_1 and MP_2 are the two measurement points.

A network measurement campaign with multiple factors and a high sampling rate is challenging and time consuming due to the large amount of measured data and the required subsequent data analysis. A DoE approach [19] was thus used to identify the different relevant configurations and limit the number of experiments. This approach creates a multi-factor design and analysis with minimum external interference by considering the different factors that contribute to the supraharmonic emissions in the test network. The selected configurations for the test network are listed in Table III. For each configuration, multiple acquisitions of fundamental and supraharmonic components of both voltage and current waveforms were performed simultaneously.

TABLE III
TEST NETWORK CONFIGURATIONS.

No.	PVI_R	PVI_I	Load	Measurement point
C_1	High	High	High	MP_1
C_2	Low	High	High	MP_1
C_3	High	Low	High	MP_1
C_4	Low	Low	High	MP_1
C_5	High	High	Low	MP_1
C_6	Low	High	Low	MP_1
C_7	High	Low	Low	MP_1
C_8	Low	Low	Low	MP_1
C_9	High	High	High	MP_2
C_{10}	Low	High	High	MP_2
C_{11}	High	Low	High	MP_2
C_{12}	Low	Low	High	MP_2
C_{13}	High	High	Low	MP_2
C_{14}	Low	High	Low	MP_2
C_{15}	High	Low	Low	MP_2
C_{16}	Low	Low	Low	MP_2

Fig. 4 shows the grid to measurement system connection. A commercial power quality analyzer (PQA) with a frequency bandwidth up to 2.5 kHz is used alongside the recorder and can be seen in Fig. 4. The PQA is used as a local control during the measurements [20]. The positional sensitivity of the RCs was ensured by positioning the conductor through the center of the coil during the measurements. In addition, the temperature and other test conditions were within the limits described in the datasheets [21-23].

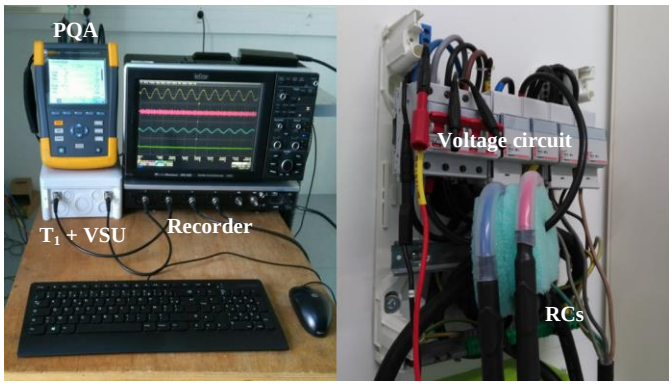

Fig. 4. Grid to measurement system connection setup (PQA - power quality analyzer, T_1 + VSU - voltage sensors, RCs - Rogowski coils).

IV. MATHEMATICAL ANALYSIS

Using the data obtained from the measurements, the FFT algorithm is used to determine the amplitude of the supraharmonic emissions in the acquired waveforms. As mentioned earlier in section II, the measured values are converted to corresponding voltage and current amplitudes using the sensitivity coefficients of the sensors. Corrections are applied for each frequency according to the sensitivity values of each channel. The measurements are broken down into multiple acquisitions of shorter time interval of 200 ms,

rather than a single long acquisition as per IEC 61000-4-7 [24].

In the following, configuration C_{10} is chosen as an example to describe the performed analysis. In configuration C_{10}, the residential PV inverter (A in Table II) is in "Low" state, which is off state and the industrial PV inverter (B) is in "High" state, which is operation in full capacity. The residential load (C) is also in "High" state, which is operation of residential equipment in full capacity. The measurement point is MP_2, which is nearby the generation equipment. The supraharmonic current emissions are shown in Fig. 5 for configuration C_{10}. This confirms the presence of supraharmonic current emissions in the test network.

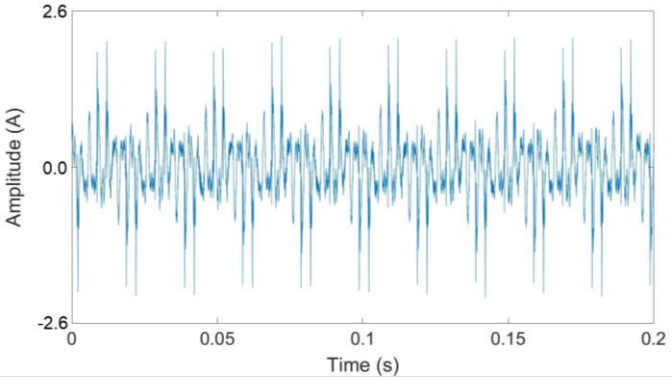

Fig. 5. RC_2 + filter measured waveform for C_{10}.

Next, Fig. 6 represents the analysis of the current waveform in the frequency range of 2 to 30 kHz for C_{10}. Significant emissions are visible in the frequency range of 2 to 10 kHz and around 20 kHz. No emissions except noise in few milliamperes are observed after 22 kHz. This indicates the absence of higher frequency emissions in this network. Nevertheless, this does not diminish the importance of higher frequency emissions detected in the other studies [1-6].

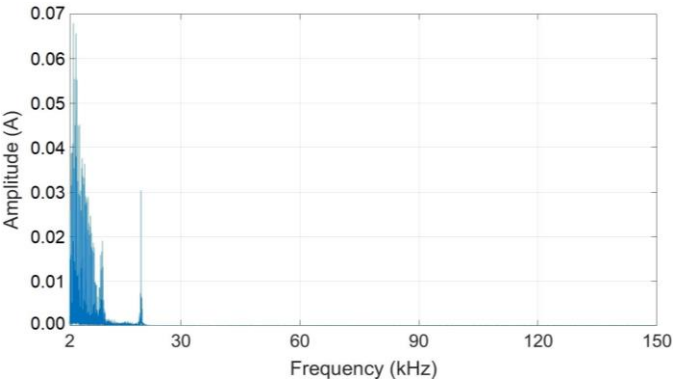

Fig. 6. RC_2 + filter measured waveform for C_{10} in frequency domain.

Mathematical analysis was performed on all the configurations listed in Table III. The supraharmonic frequency range is divided into equal intervals of 2 kHz. The peak emissions in each frequency interval are identified and quantified using the sensitivity coefficients of the sensors. The peak emissions are illustrated in Figs. 7 and 8. The analysis uses the absolute values instead of normalized values, since some of the configurations have a very low fundamental current component, e.g., C_8. In these cases, the normalized value of the emissions with respect to the fundamental current component is very high. Using the normalized values for the analysis would not yield relevant results. Therefore, the absolute value of the measured waveform enables a better comparison as the fundamental current varies over a wide range.

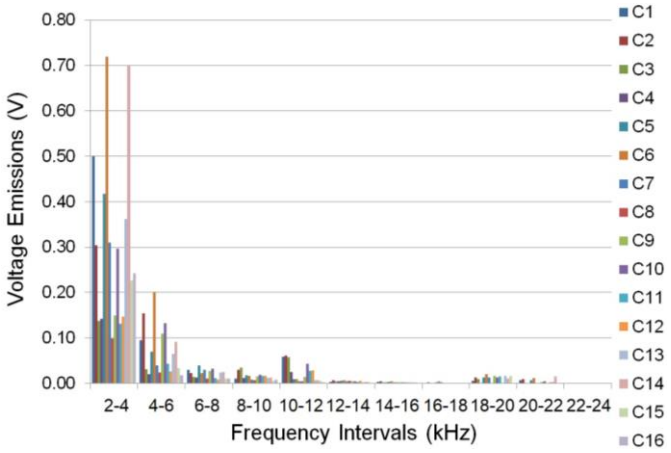

Fig. 7. Peak voltage supraharmonic emissions.

Peak voltage emissions during the network tests are shown in Fig. 7. Higher peaks are observed in the frequency range of 2 to 6 kHz, where configurations C_1, C_6, and C_{14} generate the highest peak emissions. Lower peaks are observed in the frequency range of 10 to 12 kHz. Configurations C_1, C_2, and C_3 generate the highest peak emissions in this frequency range. The industrial PV inverter (B) is in "High" state for configurations C_1 and C_2. The modes of operation of other factors vary with these configurations. This indicates the increased influence of the industrial PV inverter (B) on voltage waveform.

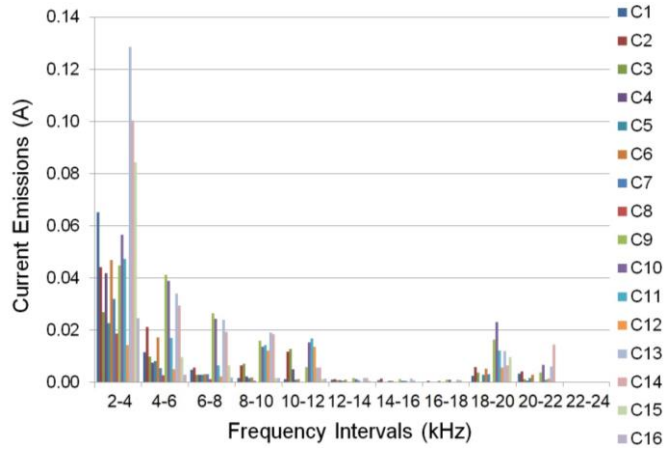

Fig. 8. Peak current supraharmonic emissions.

As for voltage, peak current emissions during the network tests are shown in Fig. 8. Higher peaks are observed in the frequency range of 2 to 4 kHz, where configurations C_{13}, C_{14}, and C_{15} generate the highest peak emissions. The residential PV inverter (A) is in "High" state for C_{13} and C_{15}. The industrial PV inverter (B) is in "High" state for C_{13} and C_{14}. Lower peaks are observed in the frequency ranges of 4 to 12 kHz, and 18 to 22 kHz. This implies that the PV inverters generate high current supraharmonics in the frequency range

of 2 to 4 kHz. From Fig. 8, it is also observed that the current emissions are higher when the measurement point (MP_2) is closer to the PV inverters. Furthermore, difference in the current emissions for the configurations, C_6 and C_{14} indicates the presence of higher emissions closer to the equipment terminal.

V. Statistical Analysis

To better analyze these results using a systematic method, a statistical analysis was used with the peak emission values obtained earlier. This statistical analysis uses ANOVA [25-27] and characterizes the individual effects and interactions between different factors in the test network. The primary and secondary emissions from the equipment during the operation are also studied. As mentioned earlier, the supraharmonic frequency range is divided into intervals of 2 kHz. There are no emissions except noise in few millivolts in the frequency range of 22 to 150 kHz. The analysis is performed on the absolute values of voltage and current supraharmonics. The frequency intervals with no visible peaks except noise are tabulated as zero. Table IV summarizes the results from the analysis and indicates the significant factors that create supraharmonic emissions in the grid. The red cells are highly significant factors, the yellow cells are significant factors, and the remaining cells are non-significant factors. These cells are individual effects and interactions between the factors, which influence the supraharmonic emissions in the test network.

TABLE IV
Effects and Interactions of Network Factors (A - Residential PV Inverter, B - Industrial PV Inverter, C - Residential Load, D - Measurement Point).

Factor	Freq. (kHz)	A	B	C	D	AB	AD	CD	BC	BD
Voltage	2 - 4									
	4 - 6									
	6 - 8									
	8 - 10									
	10 - 12									
	12 - 14									
	14 - 16									
	16 - 18									
	18 - 20									
	20 - 22									
	22 - 150									
Current	2 - 4									
	4 - 6									
	6 - 8									
	8 - 10									
	10 - 12									
	12 - 14									
	14 - 16									
	16 - 18									
	18 - 20									
	20 - 22									
	22 - 150									

From the analysis, it can be observed that the industrial PV inverter (B) is a major source of emissions, as it creates both voltage and current supraharmonics in almost the entire frequency range. The measurement point (D) also plays an important role in the network. The emissions are higher when the measurement point (D) is closer to generation equipment, which includes the residential PV inverter (A) and the industrial PV inverter (B) in comparison to other cases. The load (C) also creates supraharmonic emissions, but only in specific frequency ranges. As mentioned earlier, the load (C) is a combination of residential equipment operating at their maximum capacity. Supraharmonic current emissions during the individual operation of the residential PV inverter (A) are shown in Fig. 9. Peak emissions are in the frequency range of 2 to 4 kHz, and lower peaks are around 16 and 19.5 kHz.

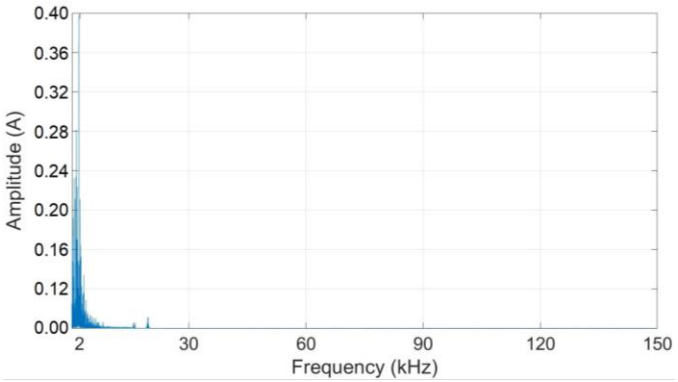

Fig. 9. RC_2 + filter measured waveform for residential PV inverter in frequency domain.

The presence of such supraharmonic emissions are detected during the individual characterization of the residential PV inverter (A), whereas in the network tests, the effects are limited to voltage emissions in the frequency range of 18 to 20 kHz. This indicates that the residential PV inverter (A) acts as a filter for the network emissions when coupled with the industrial PV inverter (B). In addition, the interactions vary with the considered waveforms, e.g., the interactions between the industrial PV inverter (B) and the load (C) are of high significance for the current but of low significance for the voltage. Furthermore, although the individual factors are significant for a particular frequency range, this does not necessarily mean that the interactions between these factors are also significant in the same frequency interval.

VI. Conclusion

The paper has described the design of a measurement system to measure the fundamental and supraharmonic components of voltage and current waveforms in the distribution network. The filtering of the fundamental components and measuring the supraharmonic components separately, maximizes the dynamic range of the recorder. The DoE approach was then used to configure the electrical network and run relevant experiments. The measurement campaign and subsequent analysis indicated different levels of supraharmonic emissions from the equipment during network and individual operation.

A statistical analysis determined the individual effects and interactions between different factors in the electrical grid during the network operation. The industrial PV inverter was

identified as the major source of supraharmonic emissions. Furthermore, some equipment was also determined to act as a filter to the emissions from other equipment during the coupled operation. Therefore, the statistical approach of analyzing the electrical network as a whole helped to better understand the effects and interactions of the factors influencing supraharmonic emissions in the distribution systems. The results from this paper can be used for the efficient modeling of electrical networks with minimum supraharmonic emissions in the frequency range of 2 to 150 kHz.

REFERENCES

[1] S. Rönnberg, M. Bollen, A. Larsson, and M. Lundmark, "An overview of the origin and propagation of Supraharmonics (2-150 kHz)," in *Proc. Nordic Conf. on Electricity Distribution System Management and Development (NORDAC)*, Stockholm, Sweden, 2014, pp. 1-12.

[2] S. Rönnberg and M. Bollen, "Power quality issues in the electric power system of the future," *The Elect. Jour.*, vol. 29, no. 10, pp. 49-61, Dec. 2016.

[3] S. Rönnberg and M. Bollen, "Measurements of primary and secondary emission in the supraharmonic frequency range 2-150 kHz," in *Proc. 23rd Int. Conf. and Exhib. on Electricity Distribution (ICEED)*, Lyon, France, 2015, pp. 1-4.

[4] C. Waniek, T. Wohlfahrt, J. M. Myrzik, J. Meyer, M. Klatt, and P. Schegner, "Supraharmonics: Root causes and interactions between multiple devices and the low voltage grid," in *Proc. IEEE PES Innovative Smart Grid Technologies Conf. (ISGT-Europe)*, Torino, Italy, 2017, pp. 1-6.

[5] S. Rönnberg, M. Bollen, and M. Wahlberg, "Interaction between narrowband power-line communication and end-user equipment," *IEEE Trans. Power Del.*, vol. 26, no. 3, pp. 2034-2039, Jul. 2011.

[6] A. Larsson and M. Bollen, "Emission and immunity of equipment in the frequency range 2 to 150 kHz," in *Proc. IEEE PowerTech*, Bucharest, Romania, 2009, pp. 1-5.

[7] L. Cristaldi, A. Ferrero, and S. Salicone, "A distributed system for electric power quality measurement," *IEEE Trans. Instrum. Meas.*, vol. 51, no. 4, pp. 776-781, Aug. 2002.

[8] S. Rönnberg, M. Bollen, and A. G. De Castro, "Harmonic distortion from energy-efficient equipment and production in the low-voltage network," Luleå Univ. of Tech., Luleå, Sweden, Res. Rep. 20141120, Aug. 2014.

[9] Electromagnetic Compatibility (EMC) - Part 4-19: Testing and measurement techniques - Test for immunity to conducted, differential mode disturbances and signalling in the frequency range 2 kHz to 150 kHz at a.c. power ports, IEC 61000-4-19, 2014.

[10] M. Klatt, J. Meyer, P. Schegner, A. Koch, J. Myrzik, T. Darda, and G. Eberl, "Emission levels above 2 kHz - laboratory results and survey measurements in public low voltage grids," in *Proc. 22nd Int. Conf. and Exhib. on Electricity Distribution (ICEED)*, Stockholm, Sweden, 2013, pp. 1-4.

[11] A. Larsson, "High frequency distortion in power grids due to electronic equipment," Licentiate thesis, Dept. Appl. Phys. and Mech. Eng., Luleå Univ. of Tech., Luleå, Sweden, 2006.

[12] D. C. Montgomery, *Design and Analysis of Experiments*, 7th ed., New Jersey, NJ, USA: J. Wiley & Sons, 2008, pp. 12-13.

[13] The Writing Studio, "Experimental and Quasi-Experimental Research," *Colorado State University*, [Online]. Available: https://writing.colostate.edu/guides/guide.cfm. [Accessed on Feb. 11, 2019].

[14] D. Amaripadath, R. Roche, L. Joseph-Auguste, D. Istrate, D. Fortuné, J. P. Braun, and F. Gao, "Measurement of supraharmonic emissions (2 - 150 kHz) in real grid scenarios," in *Proc. CPEM Conf. Dig.*, Paris, France, 2018, pp. 1-2.

[15] D. Istrate, I. Blanc, and D. Fortuné, "Development of measurement setup for high impulse currents," *IEEE Trans. Instrum. Meas.*, vol. 62, no. 6, pp. 1473-1478, Jun. 2013.

[16] B. Puluhen, "Concept grid: Préparer aujourd'hui les systèmes électriques de demain," Electricité de France, Moret-sur-Loing, France, Apr. 2015.

[17] B. Puluhen, L. Joseph-Auguste, S. Vilbois, T. Drizard, C. Lebosse, and G. Diquerreau, "Islanding tests with Li-ion storage system on the EDF concept grid," in *Proc. CIRED Workshop*, Helsinki, Finland, 2016, pp. 1-4.

[18] S. Schöttke, J. Meyer, P. Schegner, and S. Bachmann, "Emission in the frequency range of 2 kHz to 150 kHz caused by electrical vehicle charging," in *Proc. IEEE Int. Symp. on Electromagnetic Compatibility (ISEMC-Europe)*, Gothenburg, Sweden, 2014, pp. 620-625.

[19] W. G. Cochran and G. M. Cox, *Experimental Designs*, 2nd ed., New York, NY, USA: J. Wiley & Sons, 1992, pp. 1-92.

[20] A. N. Mortensen and G.L. Johnson, "A power system digital harmonic analyzer," *IEEE Trans. Instrum. Meas.*, vol. 37, no. 4, pp. 537-540, Dec. 1988.

[21] *Datasheet 44123*, Myrra, Collégien, France, 2004.

[22] *LFR Specification*, Power Electronics Measurements Ltd., Nottingham, UK, 2018.

[23] *CWT Specification*, Power Electronics Measurements Ltd., Nottingham, UK, 2018.

[24] Electromagnetic Compatibility (EMC) - Part 4-7: Testing and measurement techniques - general guide on harmonics and interharmonics measurements and instrumentation, IEC 61000-4-7, 2003.

[25] G. Zwanenburg, H. C. Hoefsloot, J. A. Westerhuis, J. J. Jansen, and A. K. Smilde, "ANOVA - principal component analysis and ANOVA - simultaneous component analysis: a comparison," *J. Chemom.*, vol. 25, no. 10, pp. 561-567, Jul. 2011.

[26] Penn State University, "Stat 502: Analysis of variance and design of experiments," *Pennsylvania State Eberly College of Science*, chap. 2. [Online]. Available: https://onlinecourses.science.psu.edu/stat502/node/137. [Accessed on Apr. 15, 2018].

[27] D. J. Sweeney, T. A. Williams, and D. R. Anderson, "Statistics science," *Encyclopedia Britannica*, chap. 7, Jul. 20, 1998. [Online]. Available: https://www.britannica.com/science/statistics. [Accessed on Apr. 16, 2018].